polymers

MDPI

Article

A Silica–Lignin Hybrid Filler in a Natural Rubber Foam Composite as a Green Oil Spill Absorbent

Yati Mardiyati [1,*], Anna Niska Fauza [1], Onny Aulia Rachman [1], Steven Steven [1] and Sigit Puji Santosa [2]

[1] Materials Science and Engineering Research Group, Faculty of Mechanical and Aerospace Engineering, Institut Teknologi Bandung, Jl. Ganesha 10, Bandung 40132, Indonesia; annaniska23@gmail.com (A.N.F.); onnyaulia7@gmail.com (O.A.R.); steven@material.itb.ac.id (S.S.)

[2] Lightweight Structure Research Group, Faculty of Mechanical and Aerospace Engineering, Institut Teknologi Bandung, Jl. Ganesha 10, Bandung 40132, Indonesia; sigit.itb@gmail.com

* Correspondence: mardiyati@material.itb.ac.id

Abstract: Oil spills in the marine environment are a rising concern due to their adverse impacts on living creatures and the environment. Hence, remediation methods have been used to remove the oil from the contaminated water. A sorbent material is considered the best method for oil spill absorption. However, commonly used commercial sorbents are made from nonrenewable and nonenvironmentally friendly materials. In this research, natural rubber foam (NRF) was used as a sorbent material with the addition of a filler, i.e., silica and a silica–lignin hybrid, to increase its oil sorption capacity and reusability. The silica and silica–lignin hybrid were extracted from rice husk waste by means of the precipitation method. The silica–lignin hybrid-filled NRF exhibited excellent hydrophobicity, with a water contact angle of 133°, and had more stable reusability compared to unfilled NRF and silica-filled NRF. In addition, the optimum oil absorption capacity of silica–lignin hybrid-filled NRF was 1.36 g g^{-1}. Overall, the results showed that silica–lignin hybrid-filled NRF has the potential to be developed as a green oil absorbent material and is promising in terms of economic and environmental aspects.

Keywords: silica-lignin hybrid; oil spill; composites; renewable absorbent material; water treatment

Citation: Mardiyati, Y.; Fauza, A.N.; Rachman, O.A.; Steven, S.; Santosa, S.P. A Silica–Lignin Hybrid Filler in a Natural Rubber Foam Composite as a Green Oil Spill Absorbent. *Polymers* **2022**, *14*, 2930. https://doi.org/10.3390/polym14142930

Academic Editors: Luigi Sorrentino and Xavier Colom

Received: 20 April 2022
Accepted: 18 July 2022
Published: 20 July 2022

1. Introduction

Oil spills in the marine environment have become a crucial issue over the last few decades. They occur due to various reasons such as offshore platforms, fuel leakages from ships, and accidents in pipelines [1]. Additionally, 5.86 million tons of oil are lost globally due to tanker accidents, according to the International Tanker Owners Pollution Federation (ITOPF) [2]. Oil spills are described as the release of hydrocarbon compounds of oil and other chemical traces (sulfur and heavy metals) by accident into the marine environment. The discharge of oil into the seawater can cause harmful impacts on the environment and interfere with the ecological system, which affects the quality of life of living organisms [3–5]. Various remediation methods have been used to remove oil in contaminated water, e.g., floating oil booms, skimmers, pumps, in situ burning, dispersants, adsorbents, and bioremediation [1]. The adsorption method is considered the most convenient method for removing oil from polluted water. A sorbent material is categorized as a wettable material with the ability to be wet or non-wet on its solid surface [6,7]. Nevertheless, commonly used materials have demonstrated low separation efficiency and poor separation selectivity [8]. Moreover, these materials are not reusable and cause secondary pollution with toxic gases and land contamination [9]. Therefore, researchers are trying to develop new materials to improve the performance of oil sorbent materials for oil spill absorption.

There are three types of wetting materials developed for oil spill absorption application: oil-removing, water-removing, and smart oil–water separation types. However, the most convenient and common type that has been developed is the oil-removing type [6].

Recently, numerous materials have been investigated for oil spill absorption application, such as graphene foam [10], a melamine sponge [11], a polyurethane sponge [12], a silica aerogel [13], polyvinyl alcohol foam [14], carbon dots/a commercial porous sponge [15], a graphene-based nanocomposite membrane [16], a biomass-based nanofiltration membrane [17], and a PEI/TMSPA/SiO_2/DTMS fabric [18]. The developed materials exhibited excellent performance and are promising for use in oil spill absorption. However, development is still in progress, despite their excellent properties, since these materials are made of nonsustainable, nonrenewable, and nonenvironmentally friendly materials. One of the promising natural materials that can be developed as a wetting material is natural rubber.

Natural rubber, which consists of cis-1,4-polyisoprene molecules, is a renewable polymer extracted from *Hevea brasiliensis* trees. It is mainly cultivated in tropical regions, such as Southeast Asia and South America [19]. Natural rubber has been widely used in engineering, medical, sports, and household applications, owing to its excellent properties. Natural rubber has good tensile and tear strength, high abrasion resistance, good hydrophobicity [20], and excellent elasticity [19]. Natural rubber has the potential to be investigated for sorbent applications due to its hydrophobic properties, especially for application in oil spill absorption. Chin et al. and Mustapa et al. studied natural rubber foam (NRF), which was a promising material for oil spill application to replace the commercial materials. Unfortunately, the results showed that the oil sorption capacity decreased due to the increase in crosslinking agents [21,22]. To improve its effectiveness, a specific material can be added to the NRF as a filler. The addition of a filler material increases the oil sorption capacity as a result of the surface roughness of the sorbent material that traps oil and other substances [23,24].

Numerous studies on the addition of filler to NRF have been conducted. Songseng et al. reported the fabrication of NRF filled with reduced graphene oxide (rGO), which generated an excellent oil sorption capacity and reusability for oil spill treatments [25]. Zou et al. studied polyethylene aerogel-coated NRF latex that had superhydrophobic and superoleophilic properties [26]. Venkatanarasimhan et al. reported the fabrication of natural rubber with the addition of magnetite nanoparticles for oil spill remediation. The material exhibited good stability and a low water uptake [27]. Riyajan et al. investigated NRF-poly(vinyl alcohol) oil sorption with biodegradable properties [28]. However, these modified oil sorbents still utilized nonrenewable and nonsustainable materials. Therefore, alternative materials are needed in order to substitute the current material used.

Recently, rice husk-based silica has been used as a sorbent in wastewater management applications because of its large surface area and active groups to bind hazardous chemicals [29,30]. The silica in rice husk is widely extracted due to its relatively high content. It is considered an economically cheap and sustainable material compared to commercial silica [31,32]. Nevertheless, according to a previous study, the silica–lignin hybrid material from rice husk has a more significant effect than silica as a sorbent due to its larger surface area and having more active sites [33]. Lignin binds to silica naturally as a matrix via hydroxyl groups. It enhances the physical sorption and acid–base interaction with other substances [34]. Therefore, the ability to absorb oil and other harmful substances is predicted to be better than silica. Furthermore, rice husk is an organic byproduct that is usually burned or wasted in the landfill. It causes harm and damage to the environment. Hence, utilizing the rice husk's composition for several applications could help prevent such things in the future [35].

To the extent of our knowledge, there is very little information regarding the utilization of the silica–lignin hybrid as a renewable filler in NRF for oil-absorbent applications. This study focuses on the effect of filler on the absorption and reusability of NRF as a sorbent material. In this research, the silica and silica–lignin hybrid were extracted from rice husk through a precipitation process. Three types of sorbent materials were prepared: unfilled NRF, silica-filled NRF, and silica–lignin hybrid-filled NRF. The results show that the silica–lignin hybrid-filled NRF is a promising material for green oil absorption.

2. Materials and Methods

2.1. Materials

Rice husk (RH) was acquired from a local paddy field in Bandung, West Java, Indonesia. Analytical grade hydrochloric acid (HCl) 37% and sulfuric acid (H_2SO_4) 96% were purchased from CV Sopyan Java Cemerlang, Bandung, Indonesia. Sodium hydroxide (NaOH) 98% was purchased from Central Kimia, Bandung, Indonesia. Ribbed smoked sheet 1 (RSS1) was obtained from PT Perkebunan Nusantara VIII, Bandung, Indonesia. Zinc oxide 93–96%, Aflux 42M, and N-cyclohexyl-2-benzothiazolesulfenamide (CBS) 98.50% were purchased from PT Multi Citra Chemindo, Jakarta, Indonesia. The azodicarbonamide blowing agent was provided by PT. Nata Kimindo Pratama, Jakarta, Indonesia. Sulfur 99.9% was obtained from CV Teja Rubber Compounding, Bandung, Indonesia.

2.2. Silica and Silica–Lignin Hybrid Extractions

Silica and silica–lignin hybrid materials were extracted using a similar procedure. Silica was extracted from the rice husk ash (RHA) precursor, whereas the silica–lignin hybrid was extracted from the rice husk (RH) precursor. RHA was prepared by a direct combustion process using a furnace at 700 °C for 6 h, whereas RH was prepared without a combustion process. The extraction process was adopted from previous reports with several modifications [34,36,37]. First, the RHA/RH was soaked in 1M of HCl solution with a ratio of 1:16 (w/v). It was reported that 1M HCl was the most effective agent in removing metallic impurities in rice husk [38]. Then, it was heated and stirred at 95 °C for 90 min. The solution was filtered using Whatman filter paper No. 93, and the residue was washed using tap water to its neutral pH and then dried overnight at room temperature. Afterward, the HCl-treated RHA/RH was mixed with 2M of NaOH solution in a ratio of 1:7 (w/v). The solution was heated and stirred at 96 °C for 4 h and then filtered using Whatman filter paper No. 93. The filtrate solution was used for the precipitation process. Then, 2M of H_2SO_4 solution was added dropwise to the filtrate solution at room temperature until pH 3–4 was reached. Furthermore, the obtained precipitate was left to stand for 6 h at room temperature and filtered with Whatman filter paper No. 93. The final residue was washed using tap water to its neutral pH and dried at 50 °C for 12 h.

2.3. Silica and Silica–Lignin Hybrid Characterizations

FTIR spectroscopy characterization was conducted to identify the functional groups of the extracted silica and silica–lignin hybrid. The FTIR Shimadzu Prestige-21 was used at the Laboratory of Analytical Chemistry, Faculty of Mathematics and Natural Sciences, Institut Teknologi Bandung, Bandung, Indonesia. The extracted silica and silica–lignin hybrid samples were mixed with KBr and then formed into a pellet. The samples were inserted into a sample holder and exposed to infrared light in the range of 400–4500 cm^{-1}.

The morphology of the extracted silica and silica–lignin hybrid was observed using a Hitachi SU3500 SEM at the Research Center of Nanoscience and Nanotechnology, Institut Teknologi Bandung, Bandung, Indonesia. The samples were prepared in an aluminum stub using adhesive tape and then coated with a layer of gold. The samples were placed into a sample holder and used for imaging. Then, the samples underwent EDX analysis and chemical analysis by exposing them to an X-ray light beam.

The morphology and characteristics of the extracted silica and silica–lignin hybrid particles were also observed using a Hitachi HT770 TEM at the Research Center of Nanoscience and Nanotechnology, Institut Teknologi Bandung, Bandung, Indonesia. The samples were prepared in a suspension form and deposited onto a carbon-coated copper grid. The samples were dried and used for imaging. Then, the samples were used for SAED pattern analysis to determine the crystal structure of the samples.

The specific surface areas of the silica and silica–lignin hybrid were analyzed using the Brunauer–Emmett–Teller (BET) method from the isotherms data via nitrogen adsorption at 77 K. Measurements were conducted using a Quantachrome instrument at the Laboratory of Analytical Instruments, Faculty of Industrial Technology, Institut Teknologi Bandung,

Bandung, Indonesia. The samples were vacuum degassed prior to the measurement process. The thermal stability of the extracted silica and silica–lignin hybrid was determined using TG/DTA characterization at the Research Center of Nanoscience and Nanotechnology, ITB, Bandung, Indonesia. The samples were placed into a sample holder with a heating rate of 10 °C/minute from 30 to 1000 °C.

2.4. Natural Rubber Compounding

The formulation used in this research is presented in Table 1. The rubber compound was prepared using an XK-160 open mill with a 1:1.35 friction ratio and 13.39 rpm roll speed. The compounding was carried out at room temperature at the Laboratory of Green Polymer, Faculty of Mechanical and Aerospace Engineering, Institut Teknologi Bandung, Bandung, Indonesia. The rubber and additives were prepared by the following procedure reported in Table 2. The samples were labeled according to the filler's type and part per hundred rubbers (phr).

Table 1. Natural rubber foam compounding formulation.

	Formulation (phr)								
	F-00	**FH-03**	**FH-05**	**FH-07**	**FH-09**	**FS-03**	**FS-05**	**FS-07**	**FS-09**
RSS1	100	100	100	100	100	100	100	100	100
Aflux 42M	2	2	2	2	2	2	2	2	2
Silica	0	0	0	0	0	3	5	7	9
Silica–lignin hybrid	0	3	5	7	9	0	0	0	0
ZnO	5	5	5	5	5	5	5	5	5
Azodicarbonamide	4	4	4	4	4	4	4	4	4
CBS	0.4	0.4	0.4	0.4	0.4	0.4	0.4	0.4	0.4
Sulfur	2	2	2	2	2	2	2	2	2

Table 2. Mixing procedure of natural rubber foam compounding formulation.

Time (min)	Action
2	Rubber mastication
4	Add Aflux 42M
8	Add fillers
2	Add CBS
4	Add ZnO
4	Add Azodicarbonamide
2	Add Sulphur
2	Homogenization

2.5. Natural Rubber Characterizations

The cure characteristics for the rubber compounds were evaluated using the MDR 2000 Alpha at the Research Center for Rubber Technology, Bogor, Indonesia. The testing temperature was 150 °C for 30 min. The torque vs. time curve was recorded to determine the scorch time (ts_2) and optimum cure time (t_{90}). It was calculated from the minimum torque (M_L) and maximum torque (M_H).

The morphologies of the NRF before and after swelling in kerosene were characterized using a Hitachi SU3500 SEM at the Research Center of Nanoscience and Nanotechnology, Institut Teknologi Bandung, Bandung, Indonesia. The samples were prepared in an aluminum stub using adhesive tape and coated with a layer of gold. The cross-section area of the NRF was observed. Then, the morphology and average cell size of the NRF were evaluated using ImageJ from the observed SEM images.

The density of the NRF was determined using a geometric method. The relative density (RD) of the NRF was calculated by dividing the density of NRF by the solid natural

rubber (0.93 g/cm^3), as shown in Equation (1). In addition, the volumetric expansion ratio (ER) was calculated as the inverse of the relative density, as shown in Equation (2) [39].

$$\text{Relative Density (RD)} = \frac{\rho_{NRF}}{\rho_{\text{solid natural rubber}}} \quad (1)$$

$$\text{Expansion ratio (ER)} = \frac{1}{\frac{\rho_{foam}}{\rho_{solid}}} \quad (2)$$

The cell size of the NRF was measured from the observed SEM image and then analyzed using the ImageJ software. Due to the anisotropic shape of the cells, their sizes were measured from two different axes: x (horizontal) and y (vertical). Twenty cells were measured from each sample and noted as average Φ_x and Φ_y.

The contact angle was measured using a digital microscope. Then, 10 µL of water was dropped from a micropipette onto a flat surface of NRF at room temperature. The image was captured and then the contact angle was determined using the Dropsnake method in the ImageJ software.

2.6. Oil Sorption Test

An oil absorption test for the NRF was conducted according to ASTM F716-09. The samples were prepared from the vulcanized rubber compound based on t_{90} data. Then, the rubber sheets were cut to a volume of 2 cm^3 and weighed using an analytical balance. The samples were immersed in 50 mL of kerosene (the viscosity was 1.6×10^{-3} Pa s, 25 °C) for 15 min. The NRF was then taken out and hung in the ambient air for 2 min (dripping time), after which it was weighed using an analytical balance. The absorption measurement was recorded as an average from three samples. The absorption capacity was calculated using Equation (3):

$$Absorption\ capacity = \left[\frac{W_2 - W_1}{W_1}\right] g\ g^{-1} \quad (3)$$

To determine its reusability, the absorption and desorption tests were repeated until the NRF was damaged. The samples were squeezed prior to the next cycle of the absorption test. The reusability of the NRF was evaluated using Equation (4) as an average from three samples:

$$Reuseability = \left[\frac{(W_2 - W_1)}{W_1}\right] g\ g^{-1} \quad (4)$$

where W_1 = weight of the unabsorbed material and W_2 = weight of the absorbed material.

3. Results and Discussion

3.1. Silica and Silica–Lignin Hybrid

3.1.1. Silica and Silica–Lignin Hybrid Extraction

Silica and silica–lignin hybrid were extracted using the precipitation method with different precursor materials. Silica was extracted from the RHA precursor through an incineration process, with the produced yield of around 16.27%. The process was conducted to remove nonsilica contents such as lignocellulose and lignin. The results showed similarities with previous reports [31,40]. Meanwhile, the silica–lignin hybrid was extracted directly from the native RH precursor without the incineration process to keep the lignin embedded within the silica. In this context, the production of the silica–lignin hybrid reduced energy consumption during the preparation process, which was more environmentally friendly compared to the production of silica material. Afterward, the precursor was pretreated with acid in order to remove trace elements such as metal oxides. Afterward, the acid-treated precursor was subjected to an alkaline treatment to separate the silica–lignin hybrid (in liquid form) from the cellulose-rich solid material. According to a previous study [37], the precipitation process was conducted at pH 3–4 due to it obtaining equal silica and lignin composition. Lignin precipitated on the silica's surface via hydrogen bonding and

increased the surface area and the active sites of the hybrid material [41]. The produced yield of the silica–lignin hybrid was around 20.53%, which was higher than the extracted pure silica. This indicated that the extraction process of the native RH precursor produced a higher content than the RHA precursor due to the presence of lignin.

3.1.2. Fourier Transform Infrared (FTIR) Spectra

The FTIR spectra showed that the silica and silica–lignin hybrid have smoother patterns compared to the other spectrum, as presented in Figure 1.

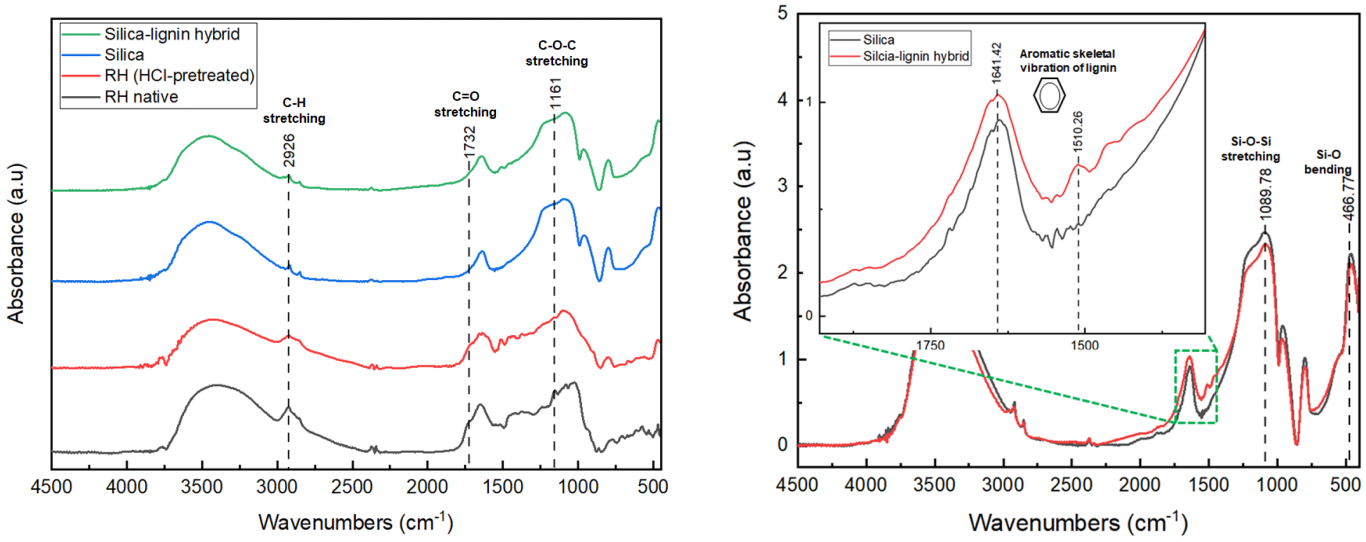

Figure 1. FTIR spectra of (**a**) RH native, RH (HCl-pretreated), silica, and silica–lignin hybrid; (**b**) the comparison peak of silica and silica–lignin hybrid.

The pattern of the FTIR spectra occurred due to the final composition of the silica and silica–lignin hybrid following the extraction process, which removed lignocellulose and other trace compositions in the RH precursor, as can be seen in Figure 1a. This was confirmed by the decrease in peak intensity at 2926 cm^{-1}, 1726 cm^{-1}, and 1163 cm^{-1}, which represented C–H stretching of the lignocellulose content, C=O stretching of hemicellulose, and C–O–C stretching of cellulose, respectively [42,43]. The silica–lignin hybrid spectra showed a strong absorption peak at 1089.78 cm^{-1}, which was assigned to Si–O–Si stretching, and 466.77 cm^{-1} to the bending vibration of Si–O. In addition, the functional group of lignin was assigned at 1641.42 cm^{-1} and 1510.26 cm^{-1}. The functional groups of the extracted silica–lignin hybrid are shown in Table 3. The difference between the silica and silica–lignin hybrid spectra is depicted in Figure 1b. The presence of lignin in the silica–lignin hybrid material was presented at the absorption peak of 1510.26 cm^{-1}. Meanwhile, the silica spectra only showed the silica-related functional groups. This was also confirmed by measurement using the Klason method (ASTM T222 om-88), which demonstrated that the silica–lignin hybrid consisted of 78.79% silica, 18.93% lignin, and 2.18% impurities.

3.1.3. Scanning Electron Microscope–Energy-Dispersive X-ray (SEM–EDX)

SEM images of the native RH, RH (HCl-pretreated), silica, and silica–lignin hybrid are shown in Figure 2. Native RH exhibited a globular structure on its surface morphology. After HCl pretreatment, it became sharper with no other significant changes, which indicated that the trace elements on the outer surface of the native RH were removed. The SEM image of the silica–lignin hybrid exhibited irregular morphology and was similar to pure silica. However, most of the silica–lignin hybrids possessed smaller particle sizes and rougher surfaces than pure silica. This indicated that lignin molecules were hydrolyzed into smaller fragments embedded onto the surface of silica.

Table 3. The functional groups of the extracted silica–lignin hybrid.

Functional Groups	Wavenumber (cm^{-1})	
	Experimental	Reference [41]
O–H stretching (silica–lignin)	3450.65	3390
C–H stretching of methyl and methylene groups	2922.16	2931
	2850.79	2881
Aromatic skeletal vibration of lignin	1641.42	1600
	1510.26	1512
Si–O–Si stretching	1089.78	1087
Si–O stretching vibration	798.53	801
Si–O bending vibration	466.77	568
Si–OH	964.41	948

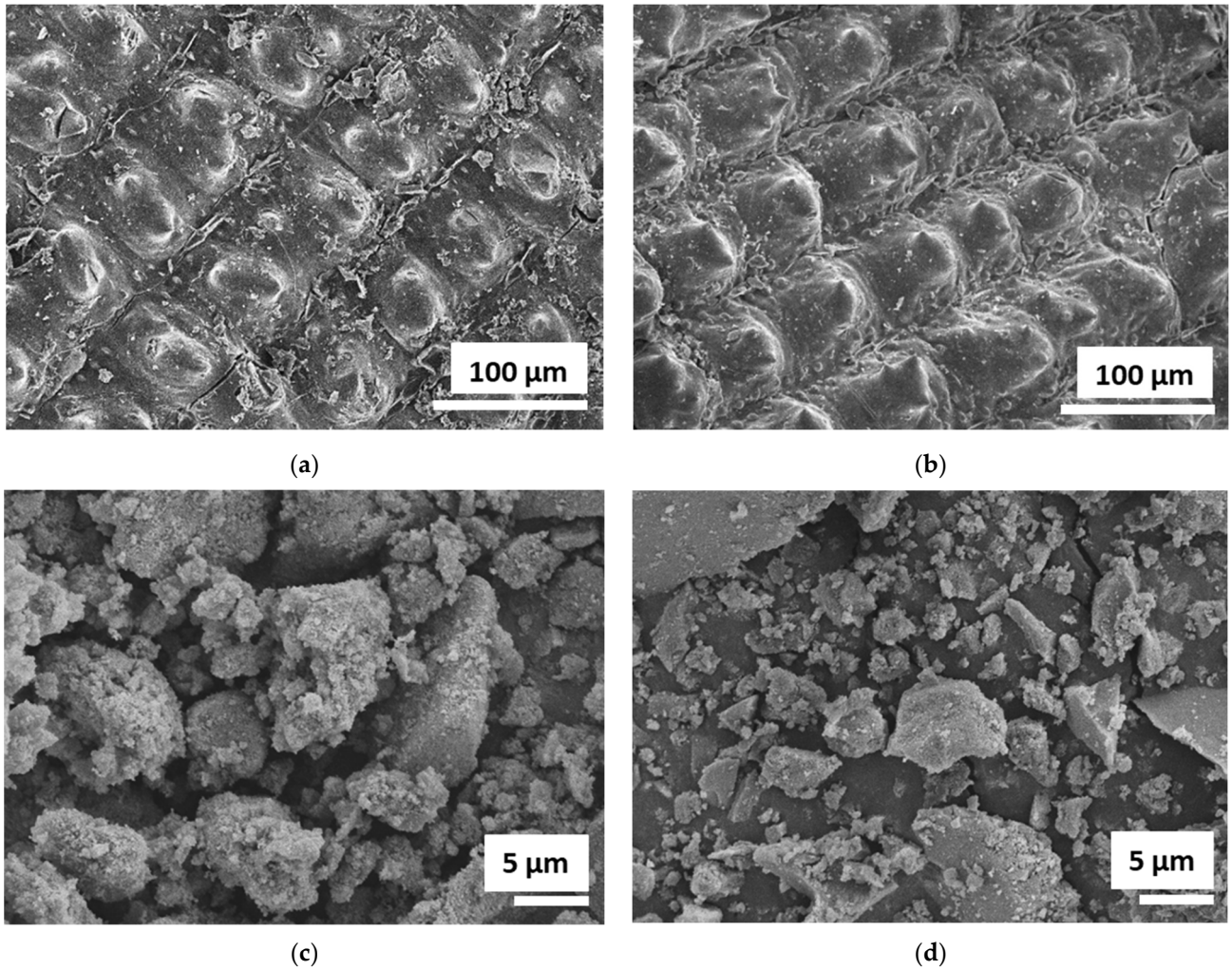

(**a**) (**b**)

(**c**) (**d**)

Figure 2. SEM images of (**a**) RH native; (**b**) RH (HCl-pretreated); (**c**) silica; and (**d**) silica–lignin hybrid.

The elemental composition of the silica and silica–lignin hybrid was determined using EDX analysis, as shown in Table 4. Both materials contain silicon, oxygen, and carbon elements. The results show that the 25.83% carbon content from the char component from RHA precursors seems to remain in the extracted silica. This was possibly due to an incomplete combustion process during the preparation of the RHA precursor [38,44]. However, the 9.51% carbon content in the silica–lignin hybrid represented the presence of lignin content as a result of the precipitation process.

Table 4. Elemental content of silica and silica–lignin hybrid based on EDX analysis.

Sample	Elemental Content (%)		
	Si	O	C
Silica	16.68	57.39	25.83
Silica–lignin hybrid	32.35	57.94	9.51

3.1.4. Transmission Electron Microscope–Selected Area Electron Diffraction (TEM–SAED)

The morphology of the silica and silica–lignin hybrid was also confirmed by TEM images, as shown in Figure 3. The results show that the silica and silica–lignin hybrid have irregular shapes with tendencies to form agglomerates. The TEM images verified that the lignin consists of small molecules embedded on the surface of silica particles. In addition, according to SAED pattern analysis, the silica and silica–lignin hybrid exhibited polycrystalline and amorphous structures, respectively.

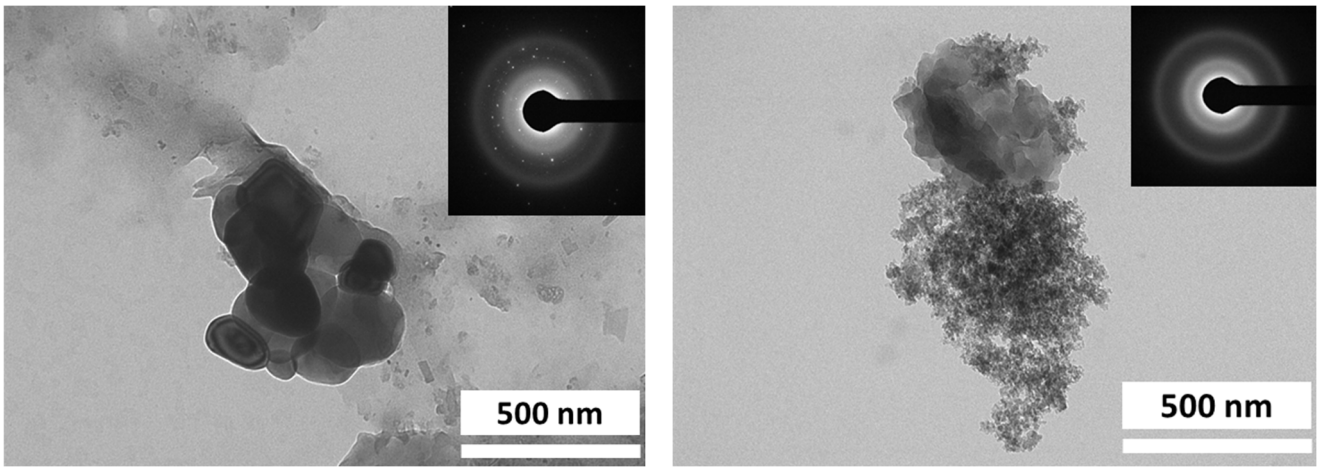

(**a**) (**b**)

Figure 3. TEM images and SAED pattern of (**a**) silica and (**b**) silica–lignin hybrid.

3.1.5. Brunauer–Emmett–Teller (BET) Analysis

The specific surface area of the silica and silica–lignin hybrid is shown in Table 5. According to the BET measurement, the results showed that the surface area of the silica–lignin hybrid was greater than that of the silica material. This confirmed that the presence of lignin had increased the surface area of the silica–lignin hybrid, which resulted in better absorption properties for the absorbent application. The previous study also showed a similar nature, which was reported by Qu et al. [34].

Table 5. Specific surface area of silica and silica–lignin hybrid using BET method analysis.

Sample	Specific Surface Area (m^2/g)
Silica	245.707
Silica–lignin hybrid	251.526

3.1.6. Thermogravimetry–Derivative Thermogravimetry (TG–DTG)

The thermal stability of the native RH, RH (HCl-pretreated), silica, and silica–lignin hybrid was determined using thermogravimetric analysis, as presented in Figure 4. The RH native and RH (HCl-pretreated) showed significant weight loss due to the removal of lignocellulose and lignin contents in the range of 260 to 370 °C and 310 to 385 °C, respectively. Up to 1000 °C, there was still 20% of weight remaining due to the un-decomposed silica content. In addition, the DTG curves of the RH and RH (HCl-pretreated) showed a

peak at 335–357 °C, which was similar to a previous report [31]. Conversely, the silica and silica–lignin hybrid have excellent thermal stability at higher temperatures. The extracted silica and silica–lignin hybrid exhibited similar characteristics in the range of 0 to 90 °C with a small weight loss from the materials. However, above 300 °C, the silica–lignin hybrid showed slightly more weight loss than the pure silica as a result of lignin decomposition.

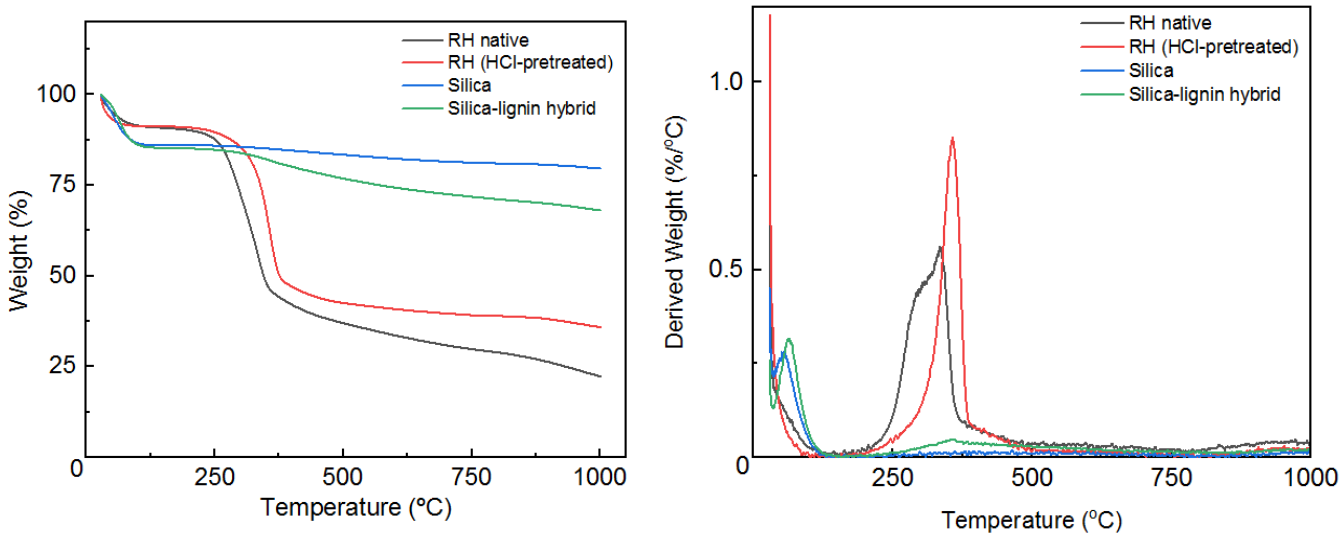

Figure 4. (**a**) Thermogravimetric analysis of RH native, RH (HCl-pretreated), silica, and silica–lignin hybrid and (**b**) DTG analysis of RH native, RH (HCl-pretreated), silica, and silica–lignin hybrid.

3.2. Natural Rubber Foam (NRF)

3.2.1. Cure Characteristics of Natural Rubber Compound

The cure curves and curing characteristics of the natural rubber compounds at 150 °C are presented in Figure 5 and Table 6, respectively. Introducing filler to the natural rubber compounds reduced the maximum torque in both the silica–lignin hybrid and silica samples. The maximum torque of natural rubber compounds decreased along with the increase in phr (part per hundred rubbers) of the filler. This was probably attributed to the decrease in the crosslink density, as indicated in the ΔS′ value. The decrease in the crosslink density was expected due to the acidic nature of both fillers. In addition, the FTIR graph showed that the silica–lignin hybrid and silica contained -OH functional groups. The acidic nature of the functional group tends to delay the vulcanization process [45]. Therefore, a lower crosslink density formed within the natural rubber compounds.

3.2.2. Density and Cellular Structure of NRF

The density and expansion ratio (ER) of the NRF are shown in Table 7. In general, most of the samples showed that the relative density increased as the addition of filler increased. The relative density of the silica–lignin hybrid-filled NRF slightly decreased for the FH-03 and FH-05 samples. This trend was also presented in silica-filled NRF. However, the decrease in density was observed in only the 3 phr sample. The increase in density was expected due to the delayed effect of the silica–lignin hybrid and silica filler during the vulcanization process—the higher the phr of filler added to the NRF, the longer the cure time. Therefore, the decomposition gas of the blowing agent was unable to be trapped inside the rubber. This was also supported by the ER data, which showed that a higher phr of filler decreased the ER value. Thus, only small fractions of cells formed inside the rubber. In this case, only FH-03, FH-05, and FS-05 exhibited an increase in ER value.

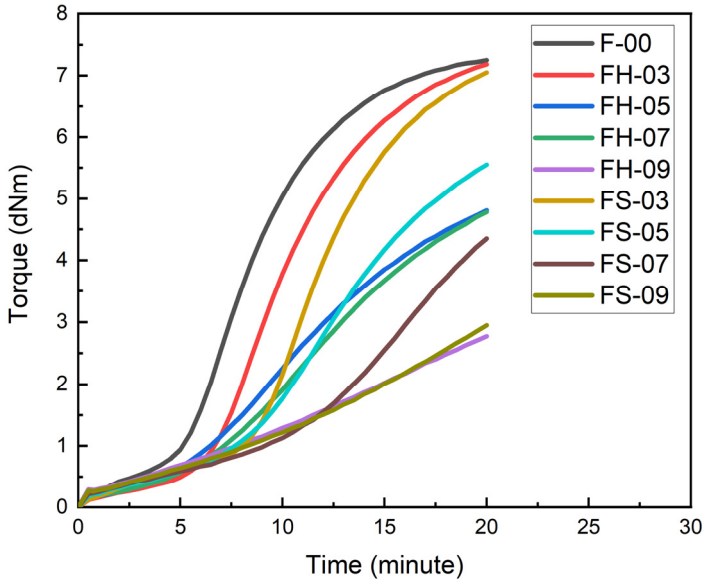

Figure 5. Cure curve of natural rubber compound at various compositions.

Table 6. Cure characteristics of natural rubber compound for various compositions at 150 °C.

Sample Code	M_L (dNm)	M_H (dNm)	ΔS′ (dNm)	t_{s2} (min)	t_{90} (min)
F-00	0.19	7.34	7.15	6.39	14.2
FH-03	0.12	7.53	7.41	8.09	17.11
FH-05	0.16	5.68	5.52	9.45	22.24
FH-07	0.17	5.78	5.61	10.4	23.04
FH-09	0.27	3.86	3.59	16.36	26.07
FS-03	0.13	7.56	7.43	9.58	18.35
FS-05	0.18	6.6	6.42	10.5	22.28
FS-07	0.22	5.96	5.74	14.06	24.57
FS-09	0.26	4.46	4.20	16.24	26.33

Table 7. Density and expansion ratio of NRF at various compositions.

Parameter	F-00	FH-03	FH-05	FH-07	FH-09	FS-03	FS-05	FS-07	FS-09
$\frac{\rho_f}{\rho_s}$	0.6099	0.5183	0.5177	0.6618	0.6746	0.5699	0.6206	0.6913	0.7786
ER	1.64	1.93	1.93	1.51	1.48	1.75	1.61	1.45	1.28
Φ_x (mm)	0.31 ± 0.15	0.36 ± 0.23	0.29 ± 0.18	0.26 ± 0.11	0.24 ± 0.007	0.25 ± 0.13	0.21± 0.12	0.26 ± 0.11	0.23 ± 0.08
Φ_y (mm)	0.79 ±0.34	0.72 ±0.27	0.51 ±0.24	0.54 ±0.22	0.38 ±0.09	0.52 ±0.28	0.33 ±0.18	0.44 ±0.17	0.36 ±0.18

The SEM images for all samples are shown in Figure 6. The NRF exhibited closed-cell foam with anisotropic cells and various cell sizes. The addition of fillers, both silica–lignin hybrid and silica, resulted in smaller cell sizes and fewer cells formed as the phr of filler increased. Therefore, more solid natural rubber formed in the samples.

3.2.3. Hydrophobicity of NRF

The hydrophobic and oleophilic characteristics of NRF were studied using water and kerosene droplets on the surface of FS-03 and FH-05 samples (Figure 7). Unfortunately, the contact angle of the kerosene droplet was unable to be determined due to the fact that the kerosene was rapidly spread and absorbed on the surface of the NRF. Nevertheless, the samples showed excellent hydrophobicity.

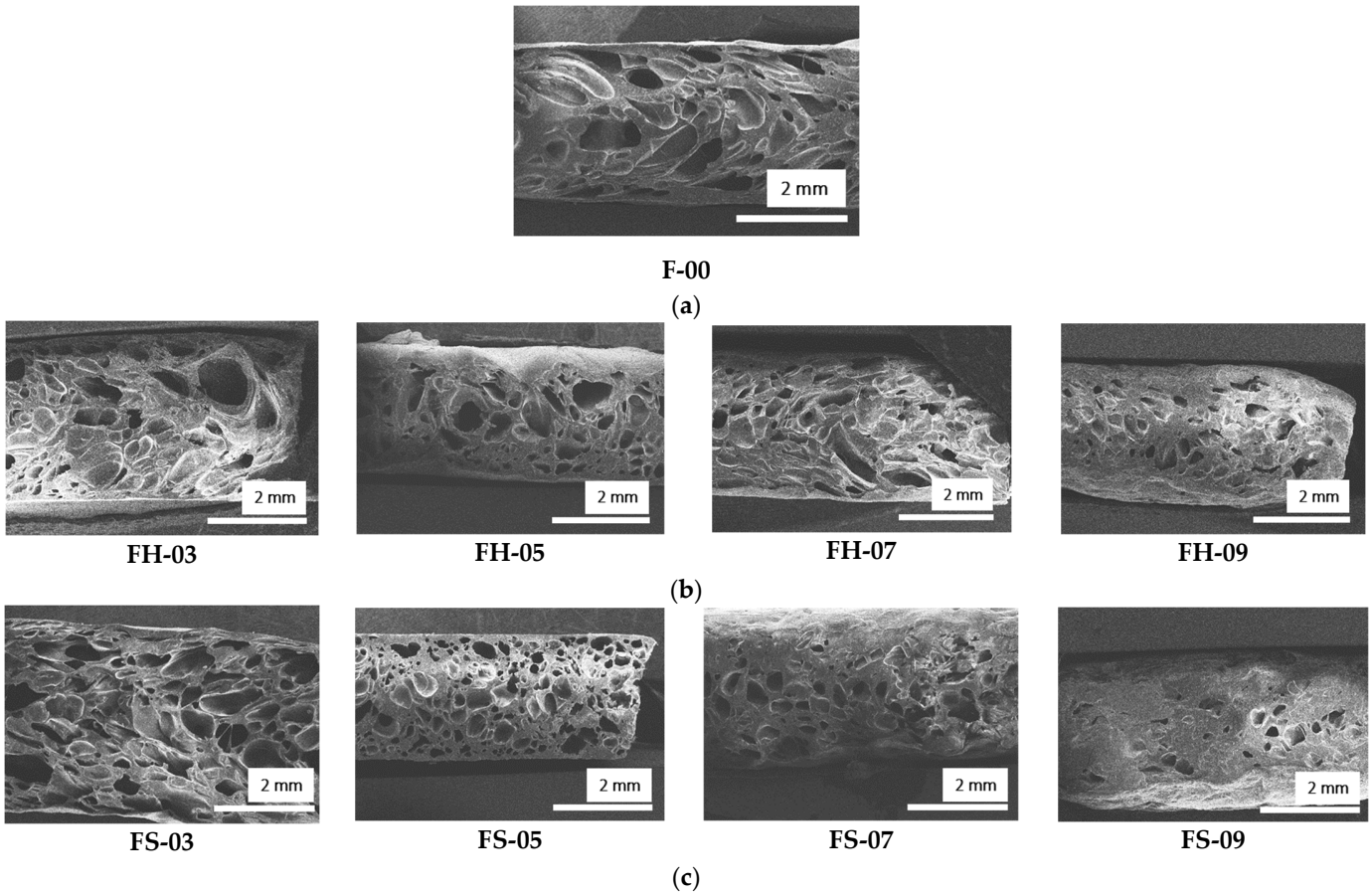

Figure 6. SEM images of (**a**) unfilled NRF; (**b**) silica–lignin hybrid-filled NRF; and (**c**) silica-filled NRF.

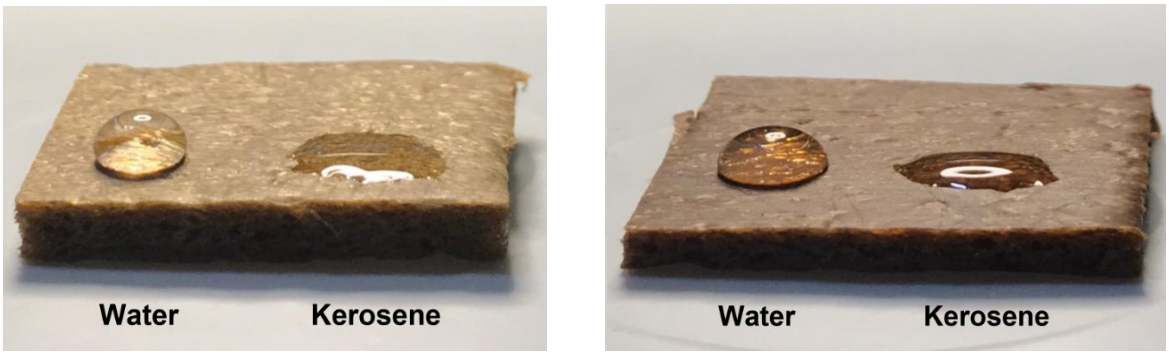

(**a**) (**b**)

Figure 7. Comparison of the contact angle of the water and kerosene on the NRF surface of (**a**) FS-03 and (**b**) FH-05 samples.

The water contact angle measurement for the NRF samples is depicted in Figure 8. The water contact angle value of the silica–lignin hybrid-filled NRF increased as the phr increased, which indicated excellent water-repellant properties. In general, the contact angle value of the samples was greater than 100°, and the highest value was 133° for sample FH-09. The unfilled NRF (F-00) sample exhibited a relatively high contact angle at a value of 110°. The value was similar to the result reported by Ratcha et al. [46], of around 117°.

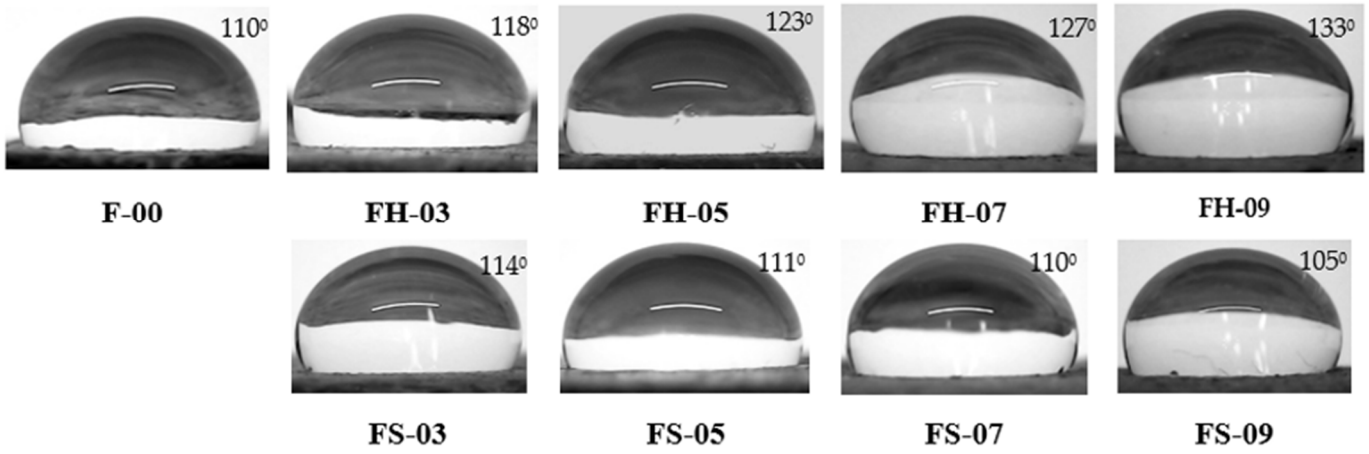

Figure 8. The contact angle of water on the NFR at various compositions.

3.2.4. Oil Absorption

The results for the oil absorption capacity using kerosene at room temperature are shown in Figure 9. The addition of filler to the NRF, both the silica–lignin hybrid and silica, led to a higher absorption capacity than unfilled NRF, except for the FS-09 sample. The absorption capacity of the NRF increased as the phr of the filler increased, and then decreased following its maximum absorption capacity. However, the silica-filled and silica–lignin hybrid-filled NRF possessed different maximum absorption capacities. Silica-filled NRF showed maximum absorption capacity at 3 phr by 1.68 g g^{-1}, and then decreased to 0.79 g g^{-1} at 9 phr. At that point, the absorption capacity was found to be lower than the unfilled NRF by 0.88 g g^{-1}. Meanwhile, the silica–lignin hybrid-filled NRF exhibited maximum absorption capacity at 5 phr by 1.36 g g^{-1}. The findings showed a similar result to the previous work reported by Chin et al. [21], which found that the absorption capacity of unfilled NRF in kerosene was in the range of 0.06–0.091 g g^{-1} per minute. In this case, the addition of filler to NRF increased the absorption capacity by 2%.

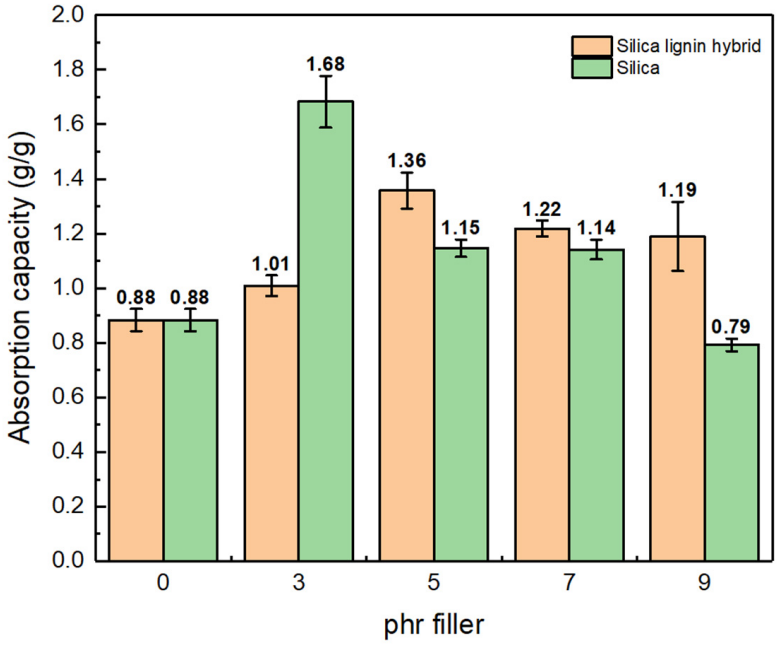

Figure 9. The first cycle of absorption capacity of silica-filled NRF and silica–lignin hybrid-filled NRF at various phr filler contents.

The oil absorption capacities of NRF depend on the cell size and the surface properties of the material [47]. The larger the cell size formed, the higher the absorption capacity of the NRF. In this case, the silica–lignin hybrid-filled NRF produced larger cell sizes compared to the silica-filled NRF. This is due to the lower density of the silica–lignin hybrid compared to silica. The foam cell can easily form and promotes the formation of large cell sizes. In addition, the presence of lignin in silica enhances the hydrophobicity of the material. Therefore, it also improves the oil absorption capacity of the NRF material.

3.2.5. Reusability of NRF

The absorption capacity at various cycles of the NRF can be seen in Figure 10. According to Figure 10b, the silica–lignin hybrid-filled NRF (FH-05) showed maximum absorption capacity by 1.36 g g^{-1} after the first cycle of exposure to kerosene. For the second cycle, the absorption capacity decreased by 0.33 g g^{-1}, which was most likely due to the residual kerosene trapped inside the pores of the NRF. Therefore, the initial weight of the NRF for the next cycle was not accurately weighed. Based on the study, the NRF can be reused 4–5 times before damage. In addition, the reusability of the silica–lignin hybrid-filled NRF was better than the silica-filled NRF.

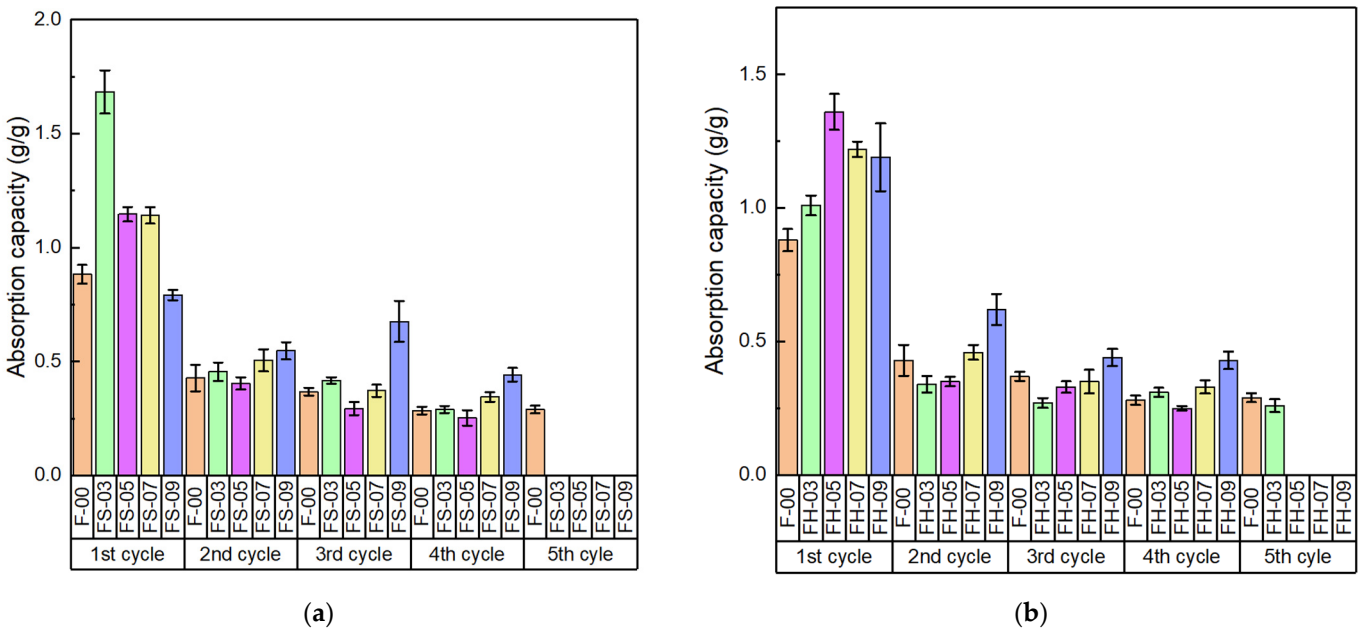

Figure 10. Absorption capacity of (**a**) silica-filled NRF and (**b**) silica–lignin hybrid-filled NRF at various cycles.

The SEM images of the NRF after the first absorption test and the last absorption test cycle are presented in Figure 11. After the oil absorption test, the shape of the cells changed into elongated shapes and more small cells appeared at the cross-section of the NRF. In addition, some of the cells collapsed, especially the cells near the surface.

3.2.6. Demonstration of Oil–Water Separation

Oil–water separation by the NRF is shown in Figure 12. The samples were immersed in a mixture of 0.7 mL blue-dyed kerosene and 15 mL tap water in a glass beaker. The samples floated on the surface of the mixture solution and successfully absorbed the oil within 15 min.

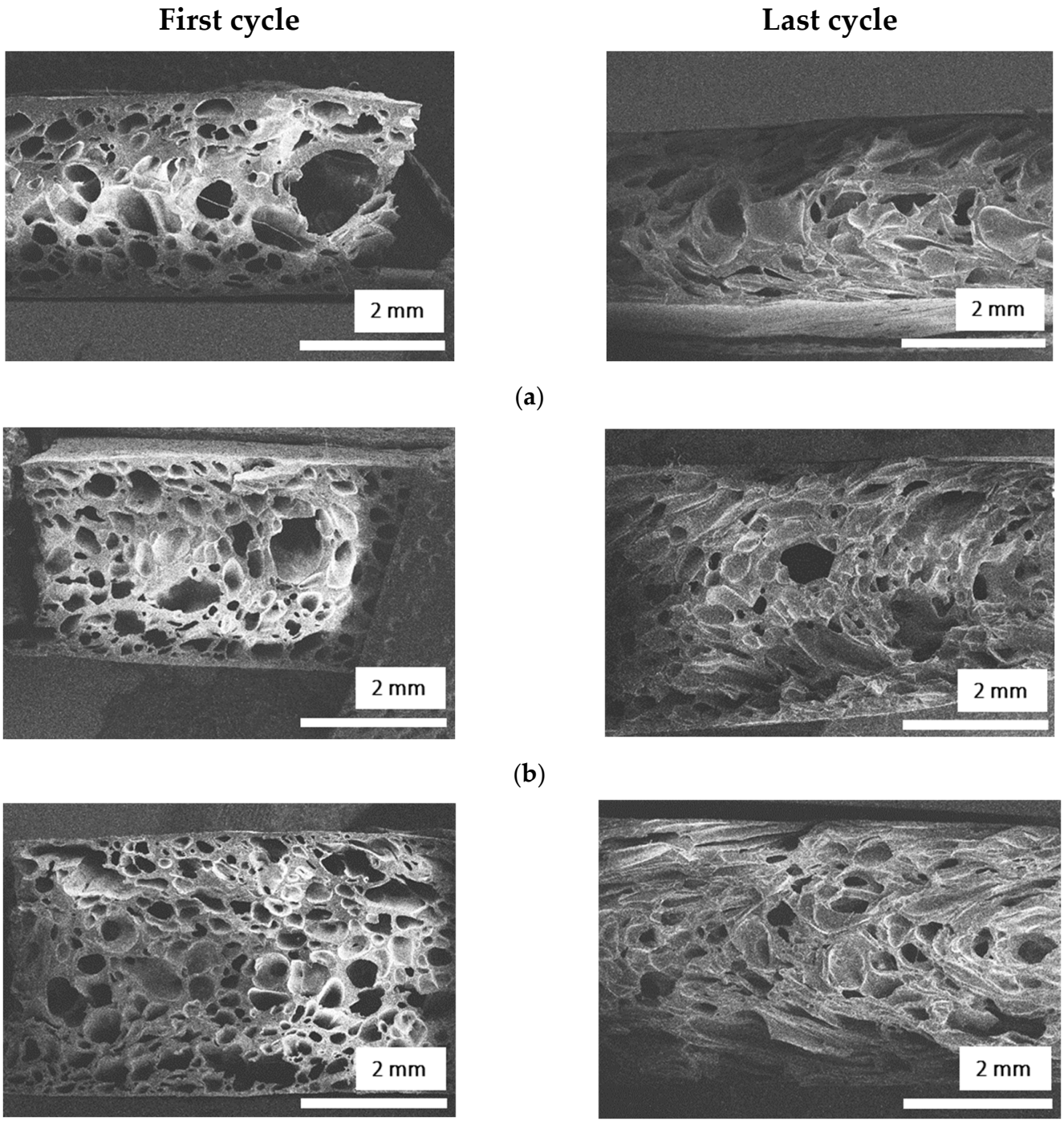

Figure 11. SEM images of NRF after the first absorption test and the last absorption test cycle: (**a**) F-00, (**b**) FH-05, and (**c**) FS-03 samples.

Based on the results above, the present work indicates that the silica–lignin hybrid-filled NRF is a promising material to substitute for the current materials used in oil spill absorption applications. In addition, it showed excellent results, especially with respect to economic and environmental factors.

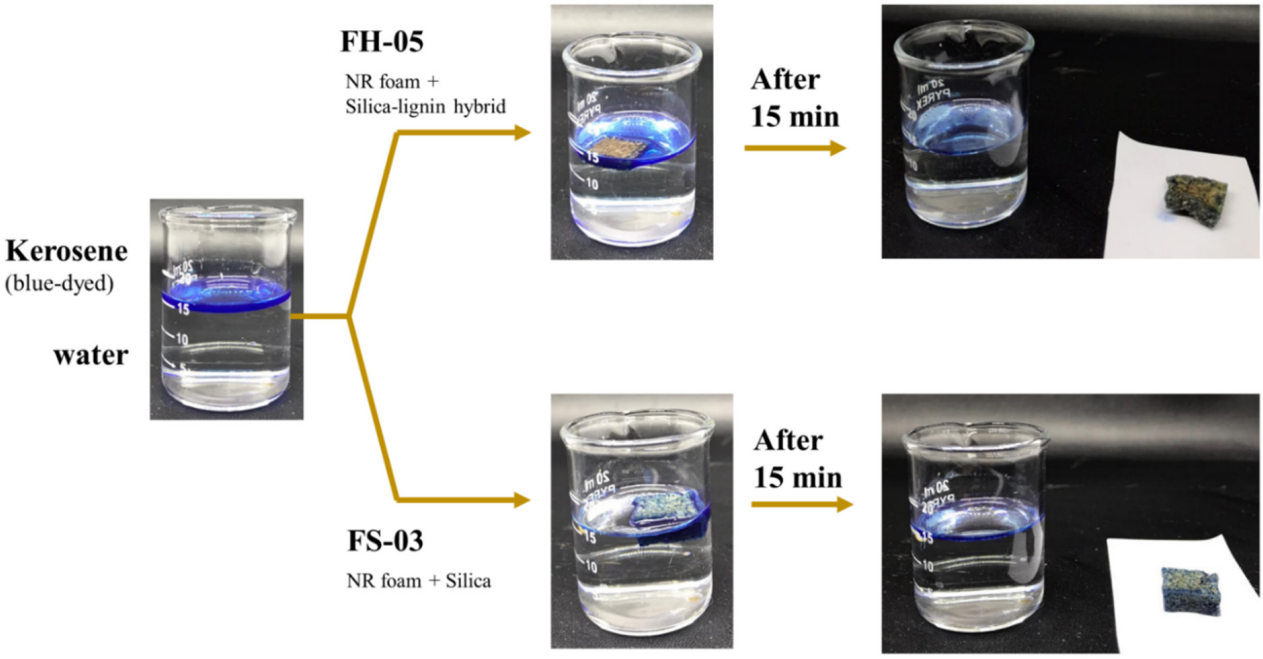

Figure 12. Demonstration of oil–water separation using the optimum silica-filled and silica–lignin hybrid-filled NRF samples.

4. Conclusions

In this study, a green oil absorbent material was developed as an alternative to the commercial ones. The addition of silica and the silica–lignin hybrid as a filler to the NRF improved the oil absorption capacity of silica-filled NRF and silica–lignin hybrid-filled NRF by 1.68 g g^{-1} and 1.36 g g^{-1} in the first cycle, respectively. Silica–lignin hybrid-filled NRF exhibited excellent hydrophobic properties, with a maximum water contact angle of 133°, as well as stable reusability. The positive results given in this research include (i) the utilization of biomass waste that is harmful to the environment, (ii) insightful ideas on using an all-natural-based material for an oil-absorption application, and (iii) promising results regarding the oil sorption properties of silica–lignin hybrid-filled NRF.

Author Contributions: Conceptualization, Y.M.; formal analysis, Y.M. and S.S.; resources, S.S.; project administration, Y.M. and S.S.; investigation, S.S., A.N.F. and O.A.R.; methodology, Y.M., A.N.F. and O.A.R.; writing—original draft preparation, A.N.F. and O.A.R.; writing—review and editing, Y.M., A.N.F. and S.P.S. All authors have read and agreed to the published version of the manuscript.

Funding: This research received no external funding.

Institutional Review Board Statement: Not applicable.

Informed Consent Statement: Not applicable.

Data Availability Statement: Data presented in this study are available on request from the corresponding author.

Acknowledgments: This research was supported by the Excellent Research Fund (Riset Unggulan ITB) from the Institute for Research and Community Service ITB (LPPM ITB). We would like to acknowledge Nata Kimindo Pratama for providing the chemical material.

Conflicts of Interest: The authors declare no conflict of interest.

References

1. Speight, J.G.; El-Gendy, N.S. Bioremediation of Marine Oil Spills. In *Introduction to Petroleum Biotechnology*; Gulf Professional Publishing: Cambridge, CA, USA, 2018; pp. 419–470. ISBN 9780128051511.
2. Oil Tanker Spill Statistics. 2019. Available online: https://www.itopf.org/fileadmin/data/Documents/Company_Lit/Oil_Spill_Stats_brochure_2020_for_web.pdf (accessed on 7 January 2021).
3. Cakir, E.; Sevgili, C.; Fiskin, R. An analysis of severity of oil spill caused by vessel accidents. *Transp. Res. Part D* **2021**, *90*, 102662. [CrossRef]
4. Zhang, B.; Matchinski, E.J.; Chen, B.; Ye, X.; Jing, L.; Lee, K. Marine Oil Spills—Oil Pollution, Sources and Effects. In *World Seas: An Environmental Evaluation*; Sheppard, C., Ed.; Academic Press: London, UK, 2019; pp. 391–406. ISBN 9780128050521.
5. Yuewen, D.; Adzigbli, L. Assessing the Impact of Oil Spills on Marine Organisms. *J. Oceanogr. Mar. Res.* **2018**, *6*, 1–7. [CrossRef]
6. Deng, Y.; Peng, C.; Dai, M.; Lin, D.; Ali, I.; Alhewairini, S.S.; Zheng, X.; Chen, G.; Li, J.; Naz, I. Recent development of super-wettable materials and their applications in oil-water separation. *J. Clean. Prod.* **2020**, *266*, 121624. [CrossRef]
7. Lin, X.; Hong, J. Recent Advances in Robust Superwettable Membranes for Oil–Water Separation. *Adv. Mater. Interfaces* **2019**, *6*, 126. [CrossRef]
8. Al-Jammal, N.; Juzsakova, T. Review of The Effectiveness of Absorbent Materials in Oil Spills Clean up. In Proceedings of the 7th International Conference of ICEEE, Budapest, Hungary, 17–19 November 2016; pp. 131–138.
9. Yong, J.; Huo, J.; Chen, F.; Yang, Q.; Hou, X. Oil/water separation based on natural materials with super-wettability: Recent advances. *Phys. Chem. Chem. Phys.* **2018**, *20*, 25140–25163. [CrossRef]
10. Liu, S.; Wang, S.; Wang, H.; Lv, C.; Miao, Y.; Chen, L.; Yang, S. Gold nanoparticles modified graphene foam with superhydrophobicity and superoleophilicity for oil-water separation. *Sci. Total Environ.* **2021**, *758*, 143660. [CrossRef]
11. Li, Z.; Guo, Z. Flexible 3D porous superhydrophobic composites for oil-water separation and organic solvent detection. *Mater. Des.* **2020**, *196*, 109144. [CrossRef]
12. Vintu, M.; Unnikrishnan, G. Indolocarbazole based polymer coated super adsorbent polyurethane sponges for oil/organic solvent removal. *J. Environ. Manag.* **2019**, *248*, 109344. [CrossRef]
13. Abolghasemi Mahani, A.; Motahari, S.; Mohebbi, A. Sol-gel derived flexible silica aerogel as selective adsorbent for water decontamination from crude oil. *Mar. Pollut. Bull.* **2018**, *129*, 438–447. [CrossRef]
14. Xi, G.Q.; Liu, T.; Ma, C.; Yuan, Q.; Xin, W.; Lu, J.J.; Ma, M.G. Superhydrophobic, compressible, and reusable polyvinyl alcohol-wrapped silver nanowire composite sponge for continuous oil-water separation. *Colloids Surf. Physicochem. Eng. Asp.* **2019**, *583*, 124028. [CrossRef]
15. Su, Y.; Chang, Q.; Xue, C.; Yang, J.; Hu, S. Solar-irradiated carbon dots as high-density hot spots in sponge for high-efficiency cleanup of viscous crude oil spill. *J. Mater. Chem.* **2022**, *10*, 585–592. [CrossRef]
16. Alammar, A.; Park, S.H.; Williams, C.J.; Derby, B.; Szekely, G. Oil-in-water separation with graphene-based nanocomposite membranes for produced water treatment. *J. Membr. Sci.* **2020**, *603*, 118007. [CrossRef]
17. Alammar, A.; Hardian, R.; Szekely, G. Upcycling agricultural waste into membranes: From date seed biomass to oil and solvent-resistant nanofiltration. *Green Chem.* **2022**, *24*, 365–374. [CrossRef]
18. Yu, H.; Wu, M.; Duan, G.; Gong, X. One-step fabrication of eco-friendly superhydrophobic fabrics for high-efficiency oil/water separation and oil spill cleanup. *Nanoscale* **2022**, *14*, 1296–1309. [CrossRef] [PubMed]
19. Kohjiya, S.; Ikeda, Y. *Chemistry, Manufacture and Applications of Natural Rubber*; Woodhead Publishing in Materials: Cambridge, UK, 2014; ISBN 9783642253874.
20. Sakdapipanich, J.T.; Rojruthai, P. Chapter 2. Natural Rubber: Biosynthesis, Structure, Properties and Application. In *Natural Rubber Materials*; RSC: London, UK, 2013; Volume 1, pp. 28–52. [CrossRef]
21. Chin, C.C.; Musbah, N.D.L.; Abdullah, I.; Lazim, A.M. Characterization and Evaluation of Prudent Liquid Natural Rubber-Based Foam for Oil Spill Control Application. *Arab. J. Sci. Eng.* **2018**, *43*, 6097–6108. [CrossRef]
22. Mustapa, M.H.; Musbah, D.L.; Muslihuddin, N.; Sulaiman, N.; Lazim, A.M. Fabrication of rubber gel as oil absorbent by using water as porosity agent for oil removal. *J. Appl. Polym. Sci.* **2019**, *136*, 47749. [CrossRef]
23. Santos, O.S.H.; Coelho da Silva, M.; Silva, V.R.; Mussel, W.N.; Yoshida, M.I. Polyurethane foam impregnated with lignin as a filler for the removal of crude oil from contaminated water. *J. Hazard. Mater.* **2017**, *324*, 406–413. [CrossRef]
24. Joy, J.; Abraham, J.; Sunny, J.; Mathew, J.; George, S.C. Hydrophobic, superabsorbing materials from reduced graphene oxide/MoS2 polyurethane foam as a promising sorbent for oil and organic solvents. *Polym. Test.* **2020**, *87*, 106429. [CrossRef]
25. Songsaeng, S.; Thamyongkit, P.; Poompradub, S. Natural rubber/reduced-graphene oxide composite materials: Morphological and oil adsorption properties for treatment of oil spills. *J. Adv. Res.* **2019**, *20*, 79–89. [CrossRef]
26. Zou, L.; Dattatray, A.; Sun, Y.; Yu, T.; Wen, S.; Xiu, Z. Superhydrophobic and superoleophilic polyethylene aerogel coated natural rubber latex foam for oil-water separation application. *Polym. Test.* **2020**, *85*, 106451. [CrossRef]
27. Venkatanarasimhan, S.; Raghavachari, D. Epoxidized natural rubber-magnetite nanocomposites for oil spill recovery. *J. Mater. Chem.* **2013**, *1*, 868–876. [CrossRef]
28. Riyajan, S.A.; Traitananan, K. Fabrication and properties of macrocellular modified natural rubber-poly (vinyl alcohol) foam for organic solvent/oil absorption. *Ind. Crops Prod.* **2020**, *153*, 112404. [CrossRef]

29. da Rosa, M.P.; Igansi, A.V.; Lütke, S.F.; Sant'anna Cadaval, T.R.; Do Santos, A.C.R.; De Oliveira Lopes Inacio, A.P.; De Almeida Pinto, L.A.; Beck, P.H. A new approach to convert rice husk waste in a quick and efficient adsorbent to remove cationic dye from water. *J. Environ. Chem. Eng.* **2019**, *7*, 103504. [CrossRef]
30. Adam, F.; Appaturi, J.N.; Khanam, Z.; Thankappan, R.; Nawi, M.A.M. Utilization of tin and titanium incorporated rice husk silica nanocomposite as photocatalyst and adsorbent for the removal of methylene blue in aqueous medium. *Appl. Surf. Sci.* **2013**, *264*, 718–726. [CrossRef]
31. Azat, S.; Korobeinyk, A.V.; Moustakas, K.; Inglezakis, V.J. Sustainable production of pure silica from rice husk waste in Kazakhstan. *J. Clean. Prod.* **2019**, *217*, 352–359. [CrossRef]
32. Chun, J.; Lee, J.H. Recent progress on the development of engineered silica particles derived from rice husk. *Sustainability* **2020**, *12*, 10683. [CrossRef]
33. Klapiszewski, L.; Jesionowski, T. Novel lignin-based materials as products for various applications. In *Handbook of Composites from Renewable Materials*; Thakur, V.K., Thakur, M.K., Kessler, M.R., Eds.; John Wiley & Sons, Inc.: Hoboken, NJ, USA, 2017; Volume 6, pp. 519–554. ISBN 9781119441632.
34. Qu, Y.; Tian, Y.; Zou, B.; Zhang, J.; Zheng, Y.; Wang, L.; Li, Y.; Rong, C.; Wang, Z. A novel mesoporous lignin/silica hybrid from rice husk produced by a sol-gel method. *Bioresour. Technol.* **2010**, *101*, 8402–8405. [CrossRef]
35. Abaide, E.R.; Tres, M.V.; Zabot, G.L.; Mazutti, M.A. Reasons for processing of rice coproducts: Reality and expectations. *Biomass Bioenergy* **2019**, *120*, 240–256. [CrossRef]
36. Yuliyati, Y.B.; Solihudin, S.; Noviyanti, A.R. Effect of Sodium Periodate on theAdsorption Capacity of Silica- Lignin from Rice Husk on Chromium(VI). *J. Kim. Sains Dan Apl.* **2019**, *22*, 242–249. [CrossRef]
37. Barana, D.; Orlandi, M.; Salanti, A.; Castellani, L.; Hanel, T.; Zoia, L. Simultaneous synthesis of cellulose nanocrystals and a lignin-silica biofiller from rice husk: Application for elastomeric compounds. *Ind. Crops Prod.* **2019**, *141*, 111822. [CrossRef]
38. Zou, Y.; Yang, T. Rice husk, rice husk ash and their applications. In *Rice Bran and Rice Bran Oil: Chemistry, Processing and Utilization*; Cheong, L.-Z., Xu, X., Eds.; Elsevier Inc.: London, UK, 2019; pp. 207–246. ISBN 9780128128282.
39. Oliveira-Salmazo, L.; Lopez-Gil, A.; Silva-Bellucci, F.; Job, A.E.; Rodriguez-Perez, M.A. Natural rubber foams with anisotropic cellular structures: Mechanical properties and modeling. *Ind. Crops Prod.* **2016**, *80*, 26–35. [CrossRef]
40. Alyosef, H.A.; Eilert, A.; Welscher, J.; Ibrahim, S.S.; Denecke, R.; Schwieger, W.; Enke, D. Characterization of biogenic silica generated by thermo chemical treatment of rice husk. *Part. Sci. Technol.* **2013**, *31*, 524–532. [CrossRef]
41. Xue, B.; Wang, X.; Yu, L.; Di, B.; Chen, Z.; Zhu, Y.; Liu, X. Self-assembled lignin-silica hybrid material derived from rice husks as the sustainable reinforcing fillers for natural rubber. *Int. J. Biol. Macromol.* **2020**, *145*, 410–416. [CrossRef] [PubMed]
42. Stuart, B.H. *Infrared Spectroscopy: Fundamentals and Applications*; John Wiley & Sons: Chichester, WS, USA, 2005; ISBN 9780470011140.
43. Yang, H.; Yan, R.; Chen, H.; Lee, D.H.; Zheng, C. Characteristics of hemicellulose, cellulose and lignin pyrolysis. *Fuel* **2007**, *86*, 1781–1788. [CrossRef]
44. Sharma, R.K.; Wooten, J.B.; Baliga, V.L.; Hajaligol, M.R. Characterization of chars from biomass-derived materials: Pectin chars. *Fuel* **2001**, *80*, 1825–1836. [CrossRef]
45. Byers, J.T. Fillers. In *Rubber Technology*; Morton, M., Ed.; Springer Science + Business Media Dordrecht: Akron, OH, USA, 1999; pp. 59–104. ISBN 9789048140107.
46. Ratcha, A.; Samart, C.; Yoosuk, B.; Sawada, H.; Reubroycharoen, P.; Kongparakul, S. Polyisoprene modified poly(alkyl acrylate) foam as oil sorbent material. *J. Appl. Polym. Sci.* **2015**, *132*, 42688. [CrossRef]
47. Lazim, A.M.; Musbah, D.L.; Chin, C.C.; Abdullah, I.; Mustapa, M.H.A.; Azfaralariff, A. Oil removal from water surface using reusable and absorptive foams via simple fabrication of liquid natural rubber (LNR). *Polym. Test.* **2019**, *73*, 39–50. [CrossRef]